UC Davis

UC Davis Previously Published Works

Title

Retinal and Choroidal Folds in PapilledemaPapilledema Folds

Permalink

https://escholarship.org/uc/item/93q9n07t

Journal

Investigative Ophthalmology & Visual Science, 56(10)

ISSN

0146-0404

Authors

Sibony, Patrick A
Kupersmith, Mark J
Feldon, Steven E
et al.

Publication Date

2015-09-03

DOI

10.1167/iovs.15-17459

Peer reviewed

eScholarship.org Powered by the California Digital Library
University of California

Retinal and Choroidal Folds in Papilledema

Patrick A. Sibony,[1] Mark J. Kupersmith,[2] Steven E. Feldon,[3] Jui-Kai Wang,[4] and Mona Garvin[4]; OCT Substudy Group for the NORDIC Idiopathic Intracranial Hypertension Treatment Trial

[1]Department of Ophthalmology, State University of New York at Stony Brook, Stony Brook, New York, United States
[2]Hyman-Newman Institute for Neurosurgery, Roosevelt Hospital, New York, New York, United States; and the New York Eye and Ear Infirmary, New York, New York, United States
[3]Department of Ophthalmology, Flaum Eye Institute, University of Rochester School of Medicine & Dentistry, Rochester, New York, United States
[4]Department of Electrical and Computer Engineering, University of Iowa, Iowa City, Iowa, United States; and Iowa City VA Health Care System, Iowa City, Iowa, United States

Correspondence: Patrick A. Sibony, Department of Ophthalmology, State University of New York at Stony Brook, Health Sciences Center, L2, Room 152, Stony Brook, NY 11794-8223, USA; patrick.Sibony@stonybrookmedicine.edu.

See the appendix for the members of the OCT Substudy Group for the NORDIC Idiopathic Intracranial Hypertension Treatment Trial.

Submitted: June 10, 2015
Accepted: July 12, 2015

Citation: Sibony PA, Kupersmith MJ, Feldon SE, Wang J-K, Garvin M; OCT Substudy Group for the NORDIC Idiopathic Intracranial Hypertension Treatment Trial. Retinal and choroidal folds in papilledema. *Invest Ophthalmol Vis Sci*. 2015;56:5670–5680. DOI:10.1167/iovs.15-17459

Purpose. To determine the frequency, patterns, associations, and biomechanical implications of retinal and choroidal folds in papilledema due to idiopathic intracranial hypertension (IIH).

Methods. Retinal and choroidal folds were studied in patients enrolled in the IIH Treatment Trial using fundus photography ($n = 165$ study eyes) and spectral-domain optical coherence tomography (SD-OCT; $n = 125$). We examined the association between folds and peripapillary shape, retinal nerve fiber layer (RNFL) thickness, disc volume, Frisén grade, acuity, perimetric mean deviation, intraocular pressure, intracranial pressure, and refractive error.

Results. We identified three types of folds in IIH patients with papilledema: peripapillary wrinkles (PPW), retinal folds (RF), and choroidal folds (CF). Frequency, with photos, was 26%, 19%, and 1%, respectively; SD-OCT frequency was 46%, 47%, and 10%. At least one type of fold was present in 41% of patients with photos and 73% with SD-OCT. Spectral-domain OCT was more sensitive. Structural parameters related to the severity of papilledema were associated with PPW and RF, whereas anterior deformation of the peripapillary RPE/basement membrane layer was associated with CF and RF. Folds were not associated with vision loss at baseline.

Conclusions. Folds in papilledema are biomechanical signs of stress/strain on the optic nerve head and load-bearing structures induced by intracranial hypertension. Folds are best imaged with SD-OCT. The patterns of retinal and choroidal folds are the products of a complex interplay between the degree of papilledema and anterior deformation of the load-bearing structures (sclera and possibly the lamina cribrosa), both modulated by structural geometry and material properties of the optic nerve head. (ClinicalTrials.gov number, NCT01003639.)

Keywords: papilledema, optical coherence tomography, optic nerve, idiopathic intracranial hypertension, choroidal folds, chorioretinal folds, peripapillary folds, retinal folds

Wrinkles and folds develop when a surface layer on a compliant substrate is exposed to a tensile, compressive, or shearing stress. They occur in a variety of structures and materials, across a wide range of scales in both inorganic materials and living tissues. The subject has been of interest to a diversity of disciplines[1–6] including ophthalmology. Nettleship[7] is credited with first recognizing choroidal folds in 1896. Since then, chorioretinal folds have been described in a variety of ophthalmic disorders including orbital and intraocular tumors; infiltrative and inflammatory diseases of the orbit, the choroid, and sclera; ocular hypotony; maculopathies; retinal detachment, scleral buckles, epiretinal membranes; microgravity space flight, among others.[6,8–10] Intracranial hypertension is a well-known cause of chorioretinal folds.[7,11–15] Folds characteristically occur in patients with papilledema, although the edema can be mild and in some cases absent.[14,15] They are typically located in the posterior pole and appear horizontal or obliquely oriented. Fluorescein angiography has been used to distinguish retinal folds from choroidal folds.[16,17] Chorioretinal folds are sometimes associated with an acquired hyperopia and posterior flattening of the globe.[12,13,15,18]

The Idiopathic Intracranial Hypertension Treatment Trial (IIHTT) was a prospective, multicenter clinical trial comparing the therapeutic efficacy of diet and acetazolamide to diet alone. The results have been reported in several publications.[19–21] The outcome measures—including the perimetric mean deviation, the severity of papilledema in the worst eye (study eye), quality of life, and intracranial pressure—improved significantly in the acetazolamide treatment group. The clinical trial also included a substudy to evaluate spectral-domain optical coherence tomography (SD-OCT) as a method of monitoring the structure of the optic nerve head in papilledema.[22,23]

The IIHTT provided high-quality fundus photos and SD-OCTs, prospectively collected using a uniform protocol with rigorous quality control evaluated by experts at reading centers. We used these images to investigate choroidal and

Copyright 2015 The Association for Research in Vision and Ophthalmology, Inc.

retinal folds in patients with IIH and papilledema. The goals of this study was to survey the frequency, types, and patterns of folds in papilledema; to correlate folds with a variety of IIH-related structural, functional, and systemic parameters; to compare fundus photography to SD-OCT in the detection of folds; and to examine the biomechanical implications of folds in papilledema.

Methods

We surveyed the baseline fundus photographs of 165 patients enrolled in the IIHTT which included 125 (76%) patients who were simultaneously enrolled in the SD-OCT substudy. The study design, patient selection, and baseline clinical profiles of the IIHTT have been published.[19–23] Briefly, patients with newly diagnosed IIH who had a perimetric mean deviation of −2.00 to −7.00 dB (Humphrey Field Analyzer II, SITA standard 24-2 test pattern; Carl Zeiss Meditec, Inc., Dublin, CA, USA), in the worse eye ("study eye") were enrolled. Standardized fundus photographs, Frisén grading of photos, best corrected high- and low-contrast visual acuity, threshold 24-2 perimetry, cerebrospinal fluid pressure, refractive error, and SD-OCT imaging (Cirrus 4000 SD-OCT, 6.01 software; Carl Zeiss Meditec, Inc.) were obtained on each patient, during each visit. Institutional review boards from each participating site approved the study. The study complied with the tenets of the Declaration of Helsinki.

All study sites followed a specific protocol for photos and SD-OCT image collection.[24] Fundus photographs were obtained from each site using a minimum of a 3-megapixel fundus camera capable of imaging a 30° to 35° field of view taken through a dilated pupil of 6 mm or larger. Each site submitted two stereo pairs of the optic discs (one pair focused on the apex of the disc and a second pair focused on the base of the disc) and one stereo pair of the macula. A scale factor based on axial length estimate and refractive error was applied to each fundus image to obtain measurements. The images were saved in uncompressed tagged image file format (TIFF) format and submitted to a reading center located at the University of Rochester for quality control and grading.[24]

Three standard OCT scans were collected: a 9-mm horizontal high-definition (HD) 5-line raster scan at 0.5-mm intervals across the central surface of the optic disc, two optic nerve head–centered volume scans; and two macula-centered volume scans. Images of the left eye were flipped horizontally to describe locations and patterns of folds in terms of the right eye. Images of OCT were uploaded for quality control by the reading center at the University of California, Davis. Images were evaluated for folds using the 5-line raster, en face imaging, and the advanced visualization analysis at specific levels of the retina for each type of fold.

Two reviewers examined the baseline fundus photos (PS, SF) and the SD-OCTs (PS, MJK) from the study eye for peripapillary wrinkles, retinal folds, and choroidal folds. Both reviewers reconciled discordant interpretations. If there was disagreement, a third reviewer determined the final designation.

Peripapillary wrinkles (PPW) were defined as periodic alternating bands on the disc surface or within a half a disc diameter onto the peripapillary retina (Fig. 1). The term wrinkles was used to designate fine, closely spaced folds around the disc. We used en face imaging at the vitreoretinal interface and axial horizontal rasters of the optic nerve head from the SD-OCT to evaluate images for PPWs. We categorized their patterns as either concentric or spiral around the optic disc. We also recorded spatial wavelength, circumferential location in clock hours (e.g., temporal 8–11 o'clock, superior 11–1, etc.), position on the disc or juxtapapillary retina, and their concurrence with retinal folds (defined below). The same determinations were made using photographs focused on the optic disc surface and the peripapillary retinal borders.

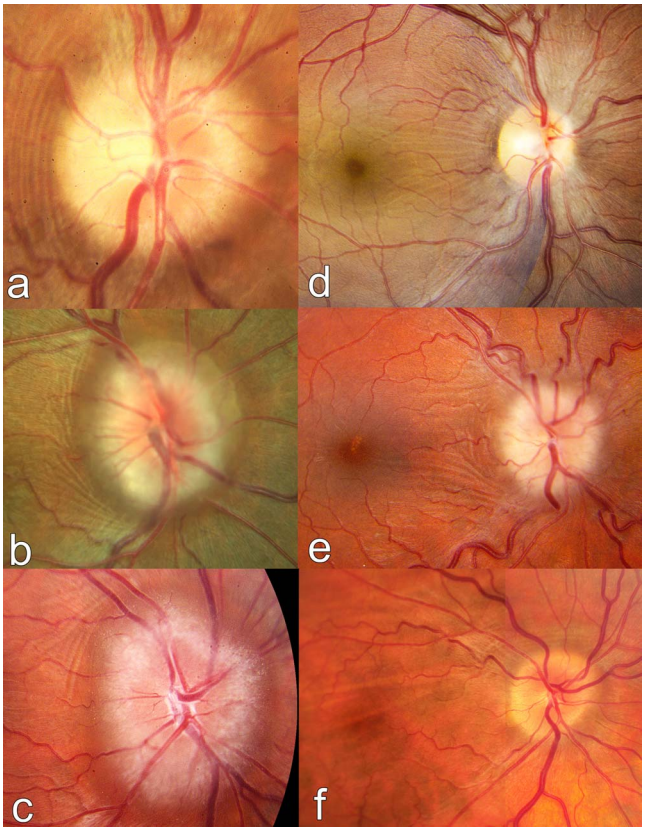

Figure 1. Fundus photographs with examples of peripapillary wrinkles, retinal folds, and choroidal folds in patients with idiopathic intracranial hypertension: (**a**) temporal concentric peripapillary wrinkles. (**b**) Inferotemporal spiral peripapillary wrinkles extending toward the macula as retinal folds. (**c**) Superotemporal spiral peripapillary wrinkles extending toward the macula. (**d**) Radial retinal folds. (**e**) Horizontal retinal folds in the papillomacular bundle. (**f**) Horizontal-oblique choroidal folds with RPE striations.

Retinal folds (RF) were defined as periodic surface or intraretinal undulations greater than half a disc diameter from the disc. We used the Advanced Visualization Analysis (optic disc and macular cubes), en face imaging at the vitreoretinal interface, and raster scans on the SD-OCT to evaluate the disc and macula for folds. Three-dimensional total thickness maps were used to confirm our interpretations. We categorized folds in terms of their orientation and patterns (e.g., horizontal, radial, oblique) and spatial frequency (peak-to-peak distance). We used a numbered early treatment diabetic retinopathy study (EDTRS) grid to record their distribution and location in the posterior pole.

Photographically, we restricted the diagnosis of choroidal folds (CF) to those patients with RF associated with deep retinal pigment epithelial striations. On the spectral-domain OCT, we required undulations in the retinal pigment epithelium/Bruch's membrane (BM) layer on the raster images and on the vertical cross sections of the macular thickness screen. Choroidal folds were described in terms of their amplitude (coarse, fine), location (using the EDTRS grid), spatial frequency, and associated RF.

We examined the association between folds and several structural and functional parameters used in the IIHTT.

Investigative Ophthalmology & Visual Science

Structural parameters included Frisén grade, total disc volume, mean retinal nerve fiber layer (RNFL) thickness, the height of the optic disc (from the RPE layer to the peak of the nerve head), and the shape of the peripapillary RPE (ppRPE)/BM layer. Functional parameters included the number of correctly identified high- and low-contrast (2.5%) visual acuity and perimetric mean deviation. We also included the best-corrected refractive error (spherical equivalent), intraocular pressure (IOP) and intracranial pressure. The methodology used to acquire each of these parameters are fully described in the main outcome studies of the clinical trial and the OCT sub study[19–25] and will not be repeated here except for a brief summary of shape analysis.

The variable characterizing the shape of the ppRPE/BM-layer was calculated using a methodology developed by Wang and Garvin.[26] The process involves a semiautomated landmark based image analysis. Using the most centrally positioned raster from the 5-line Raster OCT image, an image manipulation program (GIMP, version 2.8.10, http://www.gimp.org/, in the public domain) was used to first manually place two landmarks at the margins of Bruch's membrane opening. Automated retinal layer segmentation was used to obtain the boundaries of the internal limiting membrane and the posterior of the RPE/BM layer. Nine additional equidistant semilandmarks were automatically placed along the segmented BM/RPE boundary to provide 10 landmarks spanning 2.5 mm on the nasal and temporal side of the neural canal, which resulted in 20 total landmarks outlining the peripapillary RPE/BM boundary. Thus, the shape of the eye wall was defined by a series of equidistant landmarks positioned along the ppRPE/BM layer spanning 2500 μm on each side of the neural canal opening.[27,28] Application of a statistical shape model[26] to the 20 landmark points resulted in three coefficients that correspond to the size of Bruch's membrane opening, the RPE/BM anterior/posterior directionality, and the degree of tilt. Only anterior/posterior directionality coefficient of the RPE/BM was retained for analysis in this work. In the model, negative values represent an anterior deformation of the ppRPE/BM layer toward the vitreous and positive values describe a posteriorly oriented shape way from the vitreous.

Procrustes superimposition and principal component analysis were used to generate the statistical shape model using the 116 study eyes from the baseline IIHTT dataset.[29,26] Procrustes superimposition is a three-step process that normalizes the shape coordinates for location, scale, and rotation. Principal component analysis was used to compute the statistical shape model. In particular, the mean RPE/BM layer shape was computed followed by calculation of the eigenvectors. The principal eigenvectors with the corresponding largest three eigenvalues enables the description of each reconstructed individual shape in terms of each principal component. The coefficients that described the most relevant shape difference consisted of an anterior–posterior deformation of the ppRPE/BM layer.

Statistical Analysis

For the purposes of statistical analysis, we only included the study eye. A *t*-test was used to compare the mean Frisén score among patients with folds to the mean of those without folds. We repeated this comparison for each type of fold and each of the following variables: shape, mean RNFL, optic disc volume, height, perimetric mean deviation, visual acuity, low-contrast visual acuity, best-corrected refractive error (spherical equivalent), intracranial pressure, and intraocular pressure. The analysis was performed using SAS software (Cary, NC, USA) and P values < 0.05 were considered statistically significant. The means, standard deviations, and P values are summarized in the Table.

Results

We surveyed the fundus photographs of a 165 study eyes enrolled in the IIHTT. We reviewed the SD-OCTs of a 125 (76%) of the 165 study eyes who were also enrolled in the OCT substudy.

Fundus Photos

Forty-three (26%) study eyes had PPW, 32 (19%) had RF, and 2 (1%) had CF. In all, 68 (41%) had at least one type of fold; 7 (4%) of which had more than one type in same eye; 9 of 32 (28%) with RF and 19 (44%) of 43 with PPW were bilateral.

Peripapillary wrinkles (Figs. 1a–c) were invariably located on the temporal half of the disc and only one study eye had photographically visible folds on the nasal side. The most frequent location was just above the horizontal at 10 o'clock. The pattern was concentric in 27 (16%) and spiral in 16 (10%; 9 inferotemporal, 7 superotemporal). Ten of the study eyes with spiral PPW extended into the macula as RF.

Retinal folds (Figs. 1d, 1e) were most frequently located within the papillomacular bundle (63%). The folds were usually horizontal or slightly oblique; occasionally a radial pattern surrounding the nerve head was present. The upper hemiretina was more frequently affected than the lower hemiretina (55%:45%).

Spectral-Domain Optical Coherence Tomography

Based on review of both raster and en face imaging (Figs. 2–4), we found 58 (46%) study eyes had PPW; 59 (47%) had RF, and 13(10%) had CF. In all, 92 (73%) of study eyes exhibited at least one type of fold, 36 (29%) of which had more than one type of fold in the same eye.

Peripapillary wrinkles (Figs. 2a, 2b, 3a, 3b) were almost always located temporally between 6 and 12 o'clock; 6 (11%) also had folds located on the nasal half of the disc margin. The distribution by quadrant was 52 (93%) temporally, 30 (54%) superiorly, 32 (54%) inferiorly, and 3 (5%) nasally. Of the 58 eyes with PPW, 35 (28%) were concentric and 23 (18%) were spiral (11 inferotemporal, 12 superotemporal). Peripapillary wrinkles consisted of fine hairpin sinusoidal wrinkles confined to the retinal nerve fiber layer usually clustered at the papilloretinal inflection in 33 eyes (26%), on the temporal slope of the nerve head in 22 (18%), or on the nerve head peak in 10 (8%; Figs. 3a, 3b).

Among the 59 patients with RF there were 32 (26%) with RF oriented horizontally between the disc and fovea; 27 (22%) were radially-oriented centered on optic nerve head. There were 10 (8%) instances where macular RF were associated with spiral PPW (Figs. 2c–e, 3d, 3e).

Choroidal folds were observed in 13 (10%) study eyes (Figs. 3e–h, 4). We observed several patterns: coarse, widely-spaced folds at the level of the RPE/BM layer (Figs. 3f, 3h, 4a, 4c–e, 4h) usually associated with full thickness RF (chorioretinal folds, 7 eyes) and irregular fine undulations visible on vertically oriented cross sections through the papillomacular bundle (Figs. 3e, 3g, 6 eyes). Choroidal folds were usually, but not always, associated with overlying retinal folds (Fig. 3g). The periodicity between RF and CF was in some cases harmonic (Fig. 3f) and in others disharmonic (Fig. 3e). The coarse, widely-spaced folds were usually horizontally or obliquely oriented, located above and temporal to the nerve head in the posterior pole (Figs. 4e–h).

Investigative Ophthalmology & Visual Science

Table. Mean and Standard Deviations of Parameters in Study Eyes With and Without Folds

	Structure					Vision			Other		
	Shape	Frisén Grade	Disc Volume	RNFL	Disc Height	PMD	VA	LCVA	SE	CSF Pressure	IOP
Peripapillary wrinkles											
Mean with folds	−0.114	3.09	17.34	285	1007	−3.50	56.41	27.03	−0.92	349	15.67
SD	1.081	1.00	3.53	130	211	0.99	5.91	12.02	1.79	92	2.69
Mean without folds	−0.355	2.52	15.81	230	921	−3.48	55.64	27.10	−1.32	335	15.28
SD	1.007	1.13	3.83	138	220	1.13	5.47	10.42	2.22	75	2.42
P value	NS	**0.004**	**0.024**	**0.025**	**0.030**	NS	NS	NS	NS	NS	NS
Retinal folds											
Mean with folds	−0.697	3.11	17.92	307	1011	−3.54	55.63	26.26	−0.58	350	15.29
SD	1.027	1.03	3.84	141	227	1.13	6.52	10.78	1.85	81	2.56
Mean without folds	0.204	2.46	15.19	205	911	−3.44	56.37	27.87	−1.68	334	15.63
SD	0.863	1.09	3.16	111	202	0.99	4.71	11.52	2.07	85	2.54
P value	**<0.001**	**<0.001**	**<0.001**	**<0.001**	**0.012**	NS	NS	NS	**0.002**	NS	NS
Choroidal folds											
Mean with folds	−1.387	2.77	17.16	290	938	−3.44	55.92	24.85	−0.67	422	15.38
SD	0.982	1.01	4.13	155	214	1.17	5.48	10.17	1.90	87	2.29
Mean without folds	−0.097	2.79	16.44	251	964	−3.49	56.01	27.33	−1.19	332	15.47
SD	0.967	1.12	3.72	134	221	1.05	5.71	11.27	2.05	78	2.58
P value	**<0.001**	NS	NS	NS	NS	NS	NS	NS	NS	**<0.001**	NS

Shape variable expressed as the eigenvalue coefficient of the principal component analysis. Negative value indicates relative anterior deformation and positive value indicates relative posterior deformation of the RPE/BM layer. CSF pressure, cerebrospinal fluid opening pressure obtained at baseline with lumbar puncture with patient in the lateral decubitus position; disc height, length in microns from the RPE layer to the peak height of the optic nerve head; LCVA, low contrast visual acuity; NS, not significant; RNFL, mean retinal nerve fiber layer in microns; PMD, perimetric mean deviation; VA, visual acuity number correct; SE, best corrected refractive error expressed as a spherical equivalent. Bold *P* values are statistically significant.

Comparison of Fundus Photos to SD-OCT

The paired comparison of fundus photos to SD-OCT evaluations showed the frequency of PPW, RF, and CF for photos was 29%, 20%, and 1%, respectively; 46%, 50%, and 10%, respectively, for SD-OCT (Fig. 5). Among PPW, the results were concordant in 77% of eyes. With the exception of one eye, every discordant outcome displayed folds on OCT that was not visible in the photograph. Likewise, 70% of the RF was concordant. There were no instances where photo documented folds that were not also present on the SD-OCT.

The mean peak-to-peak distance or spatial frequency for PPW was 107 ± 20 μm; RF was 230 ± 41 μm; CF was 530 ± 111 μm.

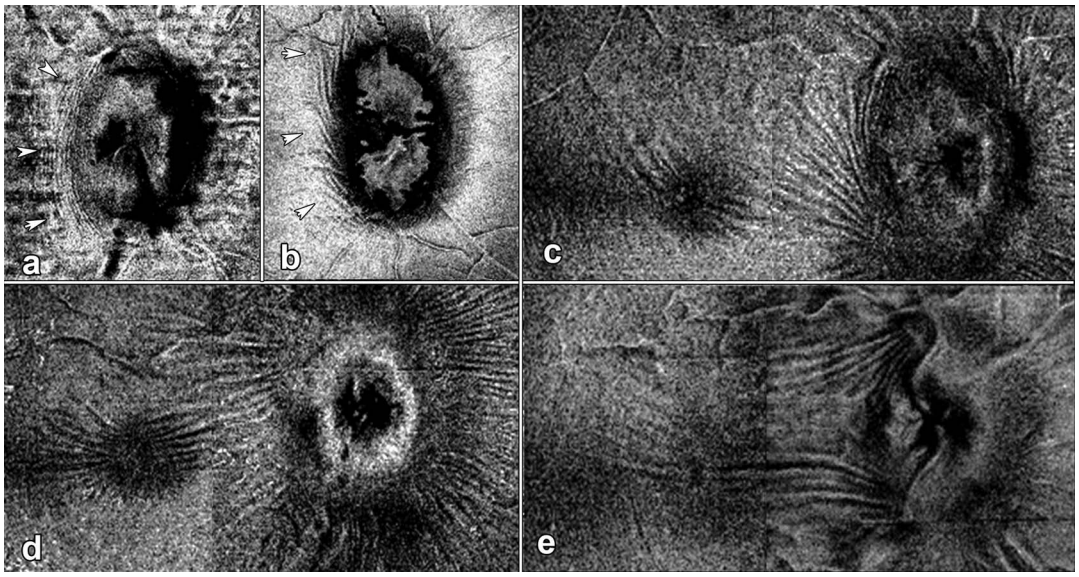

Figure 2. En face SD-OCT images at the vitreoretinal interface demonstrating peripapillary wrinkles and retinal folds in patients with idiopathic intracranial hypertension: (**a**) temporal concentric peripapillary wrinkles. (**b**) Temporal spiral peripapillary wrinkles. (**c**) Inferotemporal peripapillary spiral wrinkles extending into the macula as retinal folds. (**d**) Radial retinal folds extending into the macula. (**e**) Horizontal retinal folds in the papillomacular bundle involving the fovea.

Investigative Ophthalmology & Visual Science

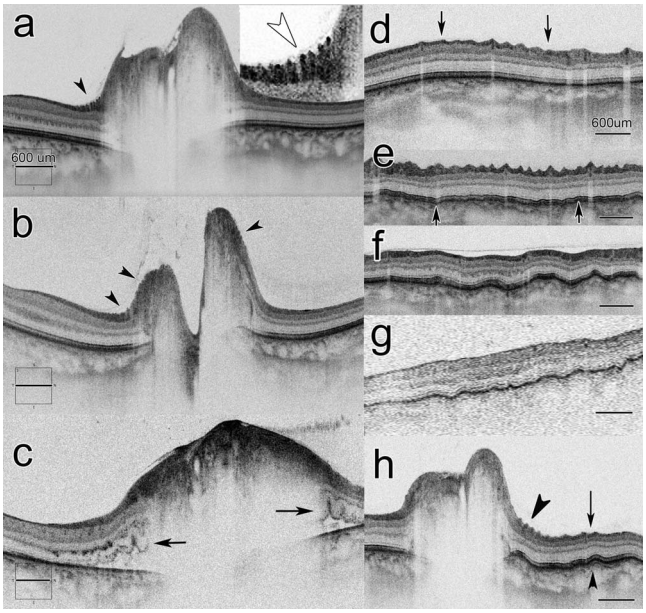

Figure 3. Axial raster images of the folds that occur in patients with idiopathic intracranial hypertension. (**a**) Optic nerve head with peripapillary wrinkles temporally confined to the nerve fiber layer at the retinopapillary inflection (*black arrowhead*). Inset magnifies that same area showing closely spaced, hairpin undulations (*white arrowhead*). (**b**) Peripapillary wrinkles on both the temporal (*double arrowheads*) and nasal side (*single arrowhead*) of the optic nerve head. (**c**) Nasal and temporal peripapillary intraretinal folds sparing the choroid and retinal surface (*black arrows*). Opposing surfaces of the folds are in contact forming a crease. Note that the spatial wavelength of the intraretinal folds is substantially wider than PPW. (**d**) Vertical (*sagittal*) raster taken through the papillomacular bundle demonstrating retinal folds (*between black arrows*) confined to the surface layers sparing outer retina and choroid. (**e**) Vertical raster exhibiting retinal folds associated with fine disharmonic choroidal undulations. (**f**) Vertical raster through the papillomacular bundle showing coarse widely spaced choroidal folds harmonically associated with surface retinal folds. (**g**) Fine choroidal folds that involve the retinal pigment epithelial layer and outer retina but spare the surface of the retina. (**h**) Axial raster showing multiple types of disharmonic folds in a single eye with peripapillary wrinkles, retinal folds and choroidal folds.

Relationship of Folds to Other Morphological and System Parameters

We compared the mean of each of the parameters among the eyes with folds to those without folds. The results are summarized in the Table. Eyes with PPW had significantly higher Frisén grades, mean RNFL thickness, optic nerve head volume and optic disc height when compared with eyes without PPW. Peripapillary wrinkles were not associated with change in shape. Choroidal folds were associated with a change in shape (i.e., anterior deformation of the peripapillary RPE/BM layer), but were not associated with any of the other structural parameters. Retinal folds had significantly higher Frisén grades, mean RNFL thickness, optic nerve head volume, and optic disc height when compared with eyes without RF. They were also associated with anterior shape deformation of the ppRPE/BM layer.

None of the fold types showed any significant difference with respect to visual acuity or perimetric mean deviation. The eyes with CF occurred in patients with significantly higher intracranial pressure than those without CF. Retinal folds were associated with significantly less myopia than without RF.

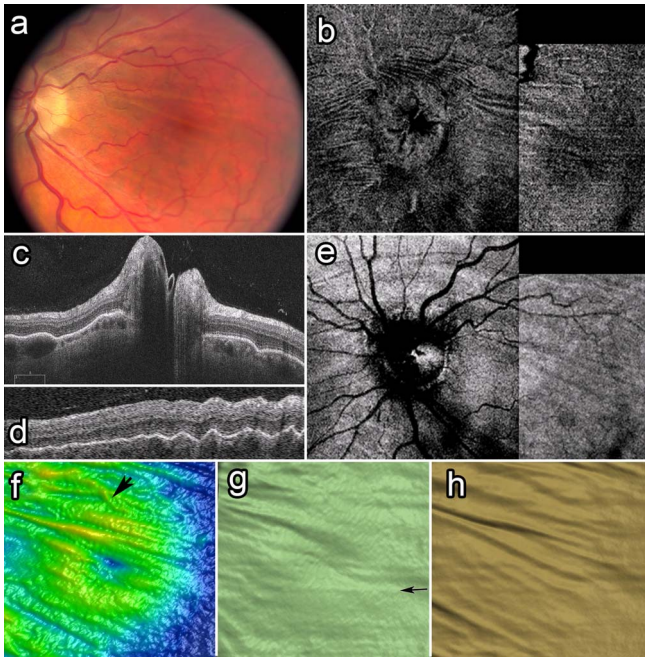

Figure 4. Multiple modalities showing OS of a patient with choroidal-retinal folds. (**a**) fundus photo demonstrating horizontal oblique chorioretinal folds with retinal pigment epithelial (RPE) striations. (**b**) En face montage at the level of the vitreoretinal interface (VRI) showing horizontal-oblique folds nasal, temporal and superior to the disc extending into the fovea. This pattern suggests a combination of tensile and compressive strain directed superiorly from the nerve head. (**c**) Axial raster image showing choroidal folds. (**d**) Cross-sectional vertical raster through the midsection of the papillomacular bundle illustrating broad full thickness harmonic chorioretinal undulations (**e**) En face montage at the level of the RPE demonstrating choroidal folds that are more widely spaced than surface layer folds in (**b**). (**f**) Three-dimensional thickness map with corresponding 3D renditions at the level of the VRI (**g**) and the RPE (**h**). *Arrow* in (**f**) shows a blood vessel and in (**g**) demonstrates horizontal line artifact due to subtle *z* axis movements of the globe or head.

Discussion

We identified three types of folds in IIH patients with papilledema: PPW, RF, and CF. Each may occur alone, but some patients may display more than one type of fold within the same eye or between eyes. Using fundus photographs, we found that 43% of the eyes displayed at least one type of fold. In contrast 73% of eyes displayed at least one type of fold by SD-OCT. The difference in frequency in part, was related to slight offsets in the photographic plane of focus, which blurred the image enough to obscure the presence of the folds. More importantly, the combination of en face, raster, and interactive features of the SD-OCT greatly enhanced our ability to identify folds and localize them to a specific layer in the retina.

In 1911, Paton[30,31] published his seminal paper on the pathology of papilledema establishing a causal connection between a "choked" disc and intracranial hypertension. In his words: "as the disc swells lateralwards, it displaces the retina ... throwing it into [a] series of folds which run concentric with the edge of the disc. This lateral bulging is due to the distension of the most peripheral nerve fibers ...." This finding is a reliable histopathological sign of papilledema. His description and photomicrographs show peripapillary intraretinal folds that spare the retinal surface and the choroid. In that same report, Paton[30] also described PPW on the fundus

Investigative Ophthalmology & Visual Science

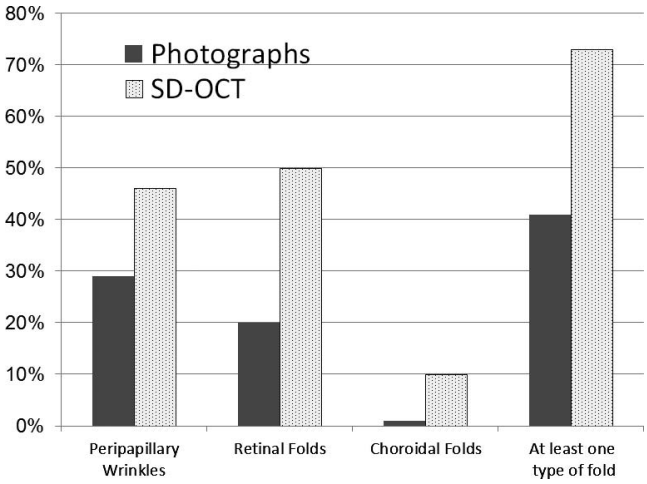

FIGURE 5. Relative frequency of folds among 125 study eyes comparing fundus photos to SD-OCT.

examination (generally referred to as "Paton's folds" or "Paton's lines").

The peripapillary intraretinal folds described by Paton histopathologically were occasionally visible on the raster images of the SD-OCT (Fig. 3c), but they were not visible photographically because they were obscured by overlying swollen opacified nerve fibers. The SD-OCT shows that PPW, seen photographically, are actually tightly spaced folds in the nerve fiber bundle layer of the optic nerve head or the juxtapapillary retina or both (Fig. 3a). They are almost always located temporally at the retinopapillary inflection but can occasionally be located at the vertical poles of the disc and rarely on the nasal side of the optic disc. Concentric PPWs do not usually extend much beyond the immediate peripapillary region, whereas the spiral wrinkles frequently extend out toward the fovea as retinal or chorioretinal folds (Figs. 1a–c, 2a–c, 3a, 3b, 4b).

Our definition of CF using fundus photos was intentionally restrictive because it is difficult to distinguish eyes with choroidal involvement in the absence of visible striations in the retinal pigment epithelium. The spectral-domain OCT is better able to determine the levels of retina involved with these folds. Retinal folds were most commonly located in the papillomacular bundle, generally horizontal or radial in pattern and occasionally associated with spiral PPW. The majority (79%) of eyes with RF did not have choroidal involvement (Figs. 1d, 1e, 2c–e, 3d, 3g, 4b).

Choroidal folds by SD-OCT were the least common type of fold (15%). Only two study eyes displayed RPE striations photographically. By spectral-domain OCT, the patterns of CF were quite variable in some cases consisting of coarse widely spaced full thickness folds (Figs. 3f, 4c–h) and in others, irregular fine undulations (Figs. 3e, 3g). In some cases, these RFs would harmonically mirror the choroidal folds (Fig. 3f) and in other cases, the periodicity between the two was disharmonic (Figs. 3e, 3h) or in one case, CFs were not associated with RFs (Fig. 3g). Choroidal folds were associated with a higher levels of intracranial pressure.

Vision based on the perimetric mean deviation, high- and low-contrast acuity was not measurably affected by the presence of retinal or choroidal folds. However, the IIHTT only included patients with mild visual impairment at study entry. The long-term consequences of folds on vision were not analyzed in this study.

The types and patterns of folds observed in this study may provide some insight into the biomechanical forces acting on the optic nerve head in patients with intracranial hypertension. Experimental and theoretical studies have shown that folds are structural instabilities of a surface layer that develop after exceeding a critical stress (force per unit area) and strain (percent deformation). Folds minimize stored elastic energy when a surface layer on a compliant substrate is compressed, extended, sheared, contracts, or expands.[1–6] Cerda and Mahadevan[5] have deduced a general theory of wrinkling and folds that includes several properties relevant to the eye. They have shown that the peak-to-peak distance (wavelength) of folds is a function of the bending stiffness; a material property based on the ratio of the modulus of elasticity of both layers, the thickness of the surface layer and Poisson's ratio. As stiffness or thickness increases, spatial wavelength widens. As strain increases beyond the critical threshold, the amplitude and area of folds increase but wavelength remains constant.

The morphological pattern of folds depends on the structural geometry of the optic nerve head and the loading force conditions. For example, uniaxial compression of a laminar structure will cause sinusoidal folds orthogonal to the vector of compression, a property that can be illustrated by pinching loose skin on the back of the hand. In contrast, a thin elastic sheet stretched lengthwise will generate folds in the same direction because tensile strain produces a perpendicular compressive stress.[5,6] Symmetrical indentation of a pressurized spherical shell produces a fixed number of radial folds that also depends on the bending stiffness.[32] Thin films subjected to torsional strains generate spiral folds.[33] Lastly, constrained volumetric growth or swelling may generate surface wrinkling.[34–36]

The wrinkles and folds in papilledema are the structural consequences of intracranial hypertension which:

1. Distends the optic nerve sheath[37];
2. Increases retrolaminar tissue pressure, which may displace the lamina cribrosa and overlying soft tissue anteriorly[30,38–40];
3. Applies a ring load at the scleral flange that anteriorly deforms the peripapillary eye wall[27,28]; and
4. Obstructs axoplasmic flow and distends the prelaminar axons, which expands the optic nerve head and displaces the juxtapapillary retina.[31,40–42]

Previous authors have speculated that choroidal folds are the result of the anterior deformation of the load bearing structures of the optic nerve head.[11,15,43] In 1974, Bullock and Egbert[44,45] showed that temporal tensile traction on the optic nerve in vivo generates horizontal choroidal-retinal folds nasal to the optic disc, an effect that was exaggerated by decreasing the intraocular pressure. They also showed that manual compression of the RPE/Bruch's membrane in cadaver eyes generates folds perpendicular to the axis of compression. Similar mechanisms have been proposed to explain the folds associated with intraconal orbital tumors.[46,47]

We found an association between the type of folds and structural parameters of the optic nerve head. Specifically, PPW were associated with higher grades of papilledema (i.e., greater mean Frisén grade, optic nerve head volume, RNFL thickness, and optic disc height), whereas CF were associated with anterior deformation of the peripapillary RPE/BM layer (shape). Retinal folds were associated with both. Choroidal folds were the only type associated with higher levels of intracranial pressure. These findings suggest that there may be at least two principal sources of stress and strain that cause folds in patients with intracranial hypertension: (1) anterior deformation of the peripapillary load bearing structures (e.g., sclera, and possibly the lamina cribrosa) and overlying soft tissues; and (2) expansive soft tissue swelling of the optic

Investigative Ophthalmology & Visual Science

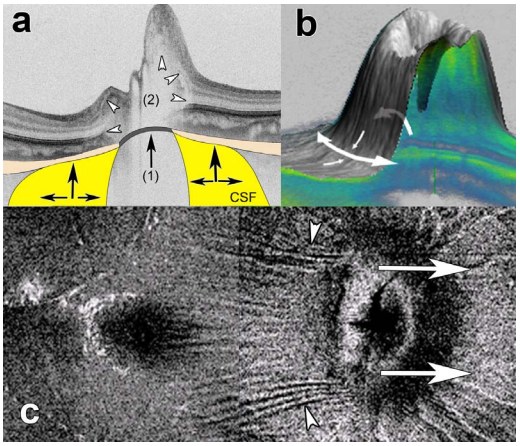

Figure 6. Biomechanical effects of intracranial hypertension on the optic nerve head (**a**) results in two principal sources of strain: (a1) anterior deformation (*black arrows*) of load bearing structures (lamina cribrosa and peripapillary sclera) and (a2) expansive soft tissue swelling of the optic nerve head. The interplay between the severity of papilledema (a2) and shape deformation (a1) modulated by individual factors related to the structural anatomy and material properties determines the pattern and distribution of the folds. (**b**) Peripapillary wrinkles may be consequent to several types of stress including intrapapillary expansive compression and circumferential hoop (tensile) stress at its base. (**c**) Horizontal folds are consequent to a tensile strain nasally that generates secondary orthogonal compression in the papillomacular bundle. Axisymmetric compression (not shown) at the scleral flange or symmetrical expansion of the nerve head might explain the radial retinal folds.

nerve head (Fig. 6). While these two forces are interrelated, their effects may be expressed independently, if not asymmetrically. Many of the IIHTT study eyes displayed only one type of fold while others showed multiple types of folds in one eye or between eyes. We have previously reported that the anterior deformation of the RPE/BM layer does not always correlate with the mean RNFL.[27] Patients with optic atrophy can exhibit anterior deformation of the ppRPE/BM layer with an increase in intracranial pressure without swelling of the nerve head.[27] Additionally, patients with intracranial hypertension may develop choroidal folds and flattening of the globe with little or no papilledema.[14,15,48] Lastly, there are many individual material and structural factors that modulate the response to these two forms of stress and strain, for example, compliance, fiber orientation and thickness of the sclera, the anatomical footprint of the scleral flange, the structural geometry of the nerve head and its insertion, and the dynamic effects of eye movements among others.[49–55]

Horizontal (nasal-temporal) RF are presumably caused by a compressive stress along the vertical (superior-inferior) axis of the globe. Because the loading forces originate at the scleral flange and optic nerve head, it is likely that these folds are induced by a temporal-nasal tensile strain as Bullock and Egbert[44,45] have suggested (Fig. 6c). In contrast, radial RFs suggest an axisymmetric indentation of the globe at the scleral flange or optic disc elevation. Peripapillary wrinkles may be consequent to both internal expansive compression and circumferential tensile hoop stress at the disc margin (Fig. 6b), particularly on the temporal side of the disc. The explanation for PPW may be more complicated because some cases appear to develop shortly after the disc edema begins to recede. Spiral PPW, particularly those extending into the macula (Fig. 2c) suggests a torsional strain, possibly due to asymmetrical focal expansion especially at the vertical poles of the disc or gaze induced torsional stress on the optic nerve head.

This study showed that each type of fold has a distinct spatial wavelength. The wavelength associated with lesions confined to the RNFL in patients with PPW was 107 ± 20 μm, whereas RF that spared the choroid measured 230 ± 41 μm and full thickness CF with retinal involvement were widely spaced at 530 ± 111 μm. The difference in wavelength of the folds of the retina and choroid is the result of a variety of factors that presumably includes weakness in appositional forces between the RNFL, outer retina, and RPE, the intrinsic material properties (bending stiffness) of each respective layer and the source of the loading forces. Delpriore[56] used these properties to show that the choroid is approximately 14-fold stiffer than the retina after controlling for thickness in patients with traction retinal and choroidal folds due to shearing. The relative spacing of folds can be used indirectly to distinguish retinal folds that spare the choroid from full thickness choroidal folds.

Left untreated, approximately 10% to 25% of patients with IIH can permanently lose vision.[57,58] While there are still some uncertainties about the relative importance of mechanical and vascular factors in vision loss, there seems little doubt that stress and strain on the optic nerve head and the load bearing structures induced by intracranial hypertension is an essential factor in the genesis of papilledema. Burgoyne et al.[50] has proposed a conceptual framework to reconcile the mechanical and vascular mechanisms in glaucoma. His paradigm views structural stress and strain on the optic nerve head as the linchpin that can adversely affect load-bearing connective tissues, blood flow, and the cellular constituents of the optic nerve head (i.e., ganglion cells, axons, glial cells, endothelial cells).[49,50,55,59,60] Notwithstanding some key biomechanical differences between glaucoma and IIH, this approach appears to be equally applicable in understanding papilledema.

There is a widely held clinical precept that the presence of folds distinguishes pathological disc edema from pseudopapilledema. We are not aware of any recent studies that have used the SD-OCT (with en face and raster images) to assess the frequency or patterns of folds in patients with pseudopapilledema; however, Carta et al.[61] assessed the frequency of folds in patients with papilledema and pseudopapilledema based on a fundus exam and photos. The study included time domain OCTs but only to evaluate the mean RNFL thickness. Among 74 patients with papilledema, 23% had folds; among 48 patients with pseudopapilledema (15 of which had optic disc drusen), none had folds. A number of studies[62–70] have used the SD-OCT to examine certain quantitative and qualitative features of pseudopapilledema with and without drusen (in some cases compared to papilledema), but none specifically commented on the presence or absence of folds. Several case reports[71–73] have described optic disc drusen associated with folds, but it is not possible to establish a causal connection between disc drusen and folds based on these cases alone. The presence of folds in a patient with optic disc drusen is usually a sign of a coincident condition (e.g., intracranial hypertension, orbital tumor) or a vascular complication of optic disc drusen (e.g., ischemic optic neuropathy, peripapillary hemorrhage, choroidal neovascular membrane).[72,74,75] We agree with Carta et. al.[61] that folds in a patient with an elevated optic disc strongly supports the diagnosis of pathological disc edema; however, at the present time we are unaware of a study that either invalidates or firmly supports the claim that it is pathognomonic.

There are several limitations in this study that should be considered. Imaging of the optic nerve with SD-OCT is prone to artifacts when the optic disc is severely swollen. The surface border of the nerve is occasionally misidentified and shadow-

ing may limit the view of the peripapillary and intrapapillary regions. There are artifacts on the 3D renditions of thickness and layers that should not be confused with folds. For example, irregular shadows caused by blood vessels can look like radial retinal folds. Additionally there are small *z*-axis movements of the eye or subject that can generate a horizontal straight line artifact (Fig. 4) that can simulate a fold. We did not perform fluorescein angiography and so it's possible that we may have underestimated the frequency of CF. Special care must be exercised when relatively simple, isotropic, structural models[1–5] are used to explain the biomechanics of a structurally complex, anisotropic structure like the optic nerve head. Nonetheless, these empirical observations can complement and inform stress and strain models of intracranial pressure on the optic nerve head using numerical methods (e.g., finite element analysis).

In summary, wrinkles and folds are common in papilledema with intracranial hypertension and consist of three basic patterns: PPW, RF, and CF. Spectral-domain OCT, specifically the raster and en face imaging, appears to be more sensitive in detecting folds than fundus photographs. Choroidal folds were the only type associated with higher levels of intracranial pressure. The presence of folds did not appear to have a measurable effect on the perimetric mean deviation and visual acuity at least in this cohort of patients. Folds are clinical manifestations of stress and strain on the optic nerve head and surrounding structures induced by intracranial hypertension. The pattern and location of folds are products of a complex interplay between the degree of papilledema and peripapillary anterior deformation of the sclera and soft tissues of the optic nerve head, both of which can be modulated by individual differences in structural anatomy and material properties of the optic nerve head. It is likely that these same forces are, to some degree, at play in all patients with intracranial hypertension and papilledema even in the absence of folds.

Acknowledgments

The authors thank Ian Sigal, PhD, for constructive comments and suggestions in preparation of the manuscript; Mary Mladek and Renee Jones for help with images; and Ann Marie Lavorna for coordinating the IRB process.

Supported in part by U10 EY017281-01A1, U10 EY017387-01A1, 3U10EY017281-01A1S1, RO1 EY023279, and an unrestricted grant from Research to Prevent Blindness (PI: SEF, MD).

Disclosure: **P.A. Sibony**, None; **M.J. Kupersmith**, None; **S.E. Feldon**, None; **J.-K. Wang**, None; **M. Garvin**, None

References

1. Genzer JG. J. Soft matter with hard skin: from skin wrinkles to templating and material characterization. *Soft Matter*. 2006;2:310–323.
2. Chung JY, Nolte AJ, Stafford CM. Surface wrinkling: a versatile platform for measuring thin-film properties. *Adv Mater*. 2011;23:3493–68.
3. Yang S, Khare, K, Lin, PC. Harnessing surface wrinkle patterns in soft matter. *Adv Funct Mater*. 2010;20:2550–2564.
4. Li B, Cao, YP, Feng, XQ, Gao, H. Mechanics of morphological instabilities and surface wrinkling in soft materials: a review. *Soft Matter*. 2012;8:5728–5745.
5. Cerda E, Mahadevan L. Geometry and physics of wrinkling. *Phys Rev Lett*. 2003;90:074302.
6. Friberg TR. The etiology of choroidal folds. A biomechanical explanation. *Graefes Arch Clin Exp Ophthalmol*. 1989;227:459–464.
7. Nettleship E. Peculiar lines in the choroid in a case of post-papillitic atrophy. *Trans Ophthalmol Soc U K*. 1884;4:167–171.
8. Weissgold DJB, Chorioretinal AJ and Retinal Folds. In: Guyer DR, Yanuzzi LA, Chang S, Shields JA, Green WR, eds. *Retina-Vitreous-Macula*. Philadelphia, PA: WB Saunders Co.; 1999:256–268.
9. Gass JDM. *Stereoscopic Atlas of Macular Diseases Diagnosis and Treatment*. St. Louis: Mosby; 1997.
10. Mader TH, Gibson CR, Pass AF, et al. Optic disc edema, globe flattening, choroidal folds, and hyperopic shifts observed in astronauts after long-duration space flight. *Ophthalmology*. 2011;118:2058–2069.
11. Bird AC, Sanders MD. Choroidal folds in association with papilloedema. *Br J Ophthalmol*. 1973;57:89–97.
12. Kalina RE, Mills RP. Acquired hyperopia with choroidal folds. *Ophthalmology*. 1980;87:44–50.
13. Dailey RA, Mills RP, Stimac GK, Shults WT, Kalina RE. The natural history and CT appearance of acquired hyperopia with choroidal folds. *Ophthalmology*. 1986;93:1336–1342.
14. Griebel SR, Kosmorsky GS. Choroidal folds associated with increased intracranial pressure. *Am J Ophthalmol*. 2000;129:513–516.
15. Jacobson DM. Intracranial hypertension and the syndrome of acquired hyperopia with choroidal folds. *J Neuroophthalmol*. 1995;15:178–185.
16. Newell FW. Fundus changes in persistent and recurrent choroidal folds. *Br J Ophthalmol*. 1984;68:32–35.
17. Norton EW. A characteristic fluorescein angiographic pattern in choroidal folds. *Proc R Soc Med*. 1969;62:119–128.
18. Stimac GK, Mills RP, Dailey RA, Shults WT, Kalina RE. CT of acquired hyperopia with choroidal folds. *AJNR Am J Neuroradiol*. 1987;8:1107–1111.
19. Wall M, Kupersmith MJ, Kieburtz KD, et al. The idiopathic intracranial hypertension treatment trial: clinical profile at baseline. *JAMA Neurol*. 2014;71:693–701.
20. NORDIC Idiopathic Intracranial Hypertension Study Group Writing Committee, Wall M, McDermott MP, et al. Effect of acetazolamide on visual function in patients with idiopathic intracranial hypertension and mild visual loss: the idiopathic intracranial hypertension treatment trial. *JAMA*. 2014;311:1641–1651.
21. Friedman DI, McDermott MP, Kieburtz K, et al. The idiopathic intracranial hypertension treatment trial: design considerations and methods. *J Neuroophthalmol*. 2014;34:107–117.
22. OCT Sub-study Committee for the NORDIC Idiopathic Intracranial Hypertension Study Group; Auinger P, Durbin M, et al. Baseline OCT measurements in the idiopathic intracranial hypertension treatment trial, part I: quality control, comparisons, and variability. *Invest Ophthalmol Vis Sci*. 2014;55:8180–8188.
23. OCT Sub-study Committee for the NORDIC Idiopathic Intracranial Hypertension Study Group; Auinger P, Durbin M, et al. Baseline OCT measurements in the idiopathic intracranial hypertension treatment trial, part II: correlations and relationship to clinical features. *Invest Ophthalmol Vis Sci*. 2014;55:8173–8179.
24. Fischer WS, Wall M, McDermott MP, Kupersmith MJ, Feldon SE; NIIHS Group. Photographic reading center of the idiopathic intracranial hypertension treatment trial (IIHTT): methods and baseline results. *Invest Ophthalmol Vis Sci*. 2015;56:3292–3303.
25. Wang JK, Kardon RH, Kupersmith MJ, Garvin MK. Automated quantification of volumetric optic disc swelling in papilledema using spectral-domain optical coherence tomography. *Invest Ophthalmol Vis Sci*. 2012;53:4069–4075.

26. Wang J-K, Sibony PA, Kardon RH, Kupersmith MJ, Garvin MK. Semi-automated 2D Bruch's membrane shape analysis in papilledema using spectral-domain optical coherence tomography. In: *Medical Imaging 2015: Biomedical Applications in Molecular, Structural, and Functional Imaging*. Vol. 9417. Orlando, FL: SPIE; 2015.
27. Sibony P, Kupersmith MJ, Honkanen R, Rohlf FJ, Torab-Parhiz A. Effects of lowering cerebrospinal fluid pressure on the shape of the peripapillary retina in intracranial hypertension. *Invest Ophthalmol Vis Sci*. 2014;55:8223–8231.
28. Sibony P, Kupersmith MJ, Rohlf FJ. Shape analysis of the peripapillary RPE layer in papilledema and ischemic optic neuropathy. *Invest Ophthalmol Vis Sci*. 2011;52:7987–7995.
29. Zelditch ML, Swiderski DL, Sheets HD, Fink WL. *Geometric Morphometrics for Biologists: a Primer*. London: Academic Press; 2004.
30. Paton LH. G. The pathology of papilledema. *Brain*. 1911;33: 389–432.
31. Paton L. Papilledema and optic neuritis: a retrospect. *Arch Ophthalmol*. 1936;15:1–20.
32. Vella D, Ajdari A, Vaziri A, Boudaoud A. Wrinkling of pressurized elastic shells. *Phys Rev Lett*. 2011;107:174301.
33. Wang J-W, Cao Y-P, Feng X-Q. Archimedean spiral wrinkles on a film-substrate system induced by torsion. *Appl Phys Lett*. 2014; 104:031910.
34. Ben Amar M, Goriely A. Growth and instability in elastic tissues. *J Mech Phys Solids*. 2005;53:2284–2319.
35. Li B, Jia F, Cao YP, Feng XQ, Gao H. Surface wrinkling patterns on a core-shell soft sphere. *Phys Rev Lett*. 2011;106:234301.
36. Volokh KY. Tissue morphogenesis: a surface buckling mechanism. *Int J Dev Biol*. 2006;50:359–365.
37. Brodsky MC, Vaphiades M. Magnetic resonance imaging in pseudotumor cerebri. *Ophthalmology*. 1998;105:1686–1693.
38. Morgan WH, Chauhan BC, Yu DY, Cringle SJ, Alder VA, House PH. Optic disc movement with variations in intraocular and cerebrospinal fluid pressure. *Invest Ophthalmol Vis Sci*. 2002; 43:3236–3242.
39. Morgan WH, Yu DY, Alder VA, et al. The correlation between cerebrospinal fluid pressure and retrolaminar tissue pressure. *Invest Ophthalmol Vis Sci*. 1998;39:1419–1428.
40. Hayreh SS. Optic disc edema in raised intracranial pressure. V. Pathogenesis. *Arch Ophthalmol*. 1977;95:1553–1565.
41. Tso MO, Hayreh SS. Optic disc edema in raised intracranial pressure. III. A pathologic study of experimental papilledema. *Arch Ophthalmol*. 1977;95:1448–1457.
42. Tso MO, Hayreh SS. Optic disc edema in raised intracranial pressure. IV. Axoplasmic transport in experimental papilledema. *Arch Ophthalmol*. 1977;95:1458–1462.
43. Cassidy LM, Sanders MD. Choroidal folds and papilloedema. *Br J Ophthalmol*. 1999;83:1139–1143.
44. Bullock JD, Egbert PR. Experimental choroidal folds. *Am J Ophthalmol*. 1974;78:618–623.
45. Bullock JD, Egbert PR. The origin of choroidal folds - a clinical, histopathological and experimental study. *Doc Ophthalmol*. 1974;2:261–263.
46. Friberg TR, Grove AS Jr. Choroidal folds and refractive errors associated with orbital tumors. An analysis. *Arch Ophthalmol*. 1983;101:598–603.
47. Wolter JR. Parallel horizontal choroidal folds secondary to an orbital tumor. *Am J Ophthalmol*. 1974;77:669–673.
48. Sanders MD. The Bowman Lecture. Papilloedema: 'the pendulum of progress'. *Eye (Lond)*. 1997;11(pt 3):267–294.
49. Downs JC, Roberts MD, Burgoyne CF. Mechanical environment of the optic nerve head in glaucoma. *Optom Vis Sci*. 2008;85: 425–435.
50. Burgoyne CF, Downs JC, Bellezza AJ, Suh JK, Hart RT. The optic nerve head as a biomechanical structure: a new paradigm for understanding the role of IOP-related stress and strain in the pathophysiology of glaucomatous optic nerve head damage. *Prog Retin Eye Res*. 2005;24:39–73.
51. Sigal IA, Flanagan JG, Ethier CR. Factors influencing optic nerve head biomechanics. *Invest Ophthalmol Vis Sci*. 2005; 46:4189–4199.
52. Sigal IA, Flanagan JG, Tertinegg I, Ethier CR. Modeling individual-specific human optic nerve head biomechanics. Part I: IOP-induced deformations and influence of geometry. *Biomech Model Mechanobiol*. 2009;8:85–98.
53. Sigal IA, Flanagan JG, Tertinegg I, Ethier CR. Modeling individual-specific human optic nerve head biomechanics. Part II: influence of material properties. *Biomech Model Mechanobiol*. 2009;8:99–109.
54. Sigal IA, Flanagan JG, Tertinegg I, Ethier CR. Predicted extension, compression and shearing of optic nerve head tissues. *Exp Eye Res*. 2007;85:312–322.
55. Sigal IA, Flanagan JG, Tertinegg I, Ethier CR. Finite element modeling of optic nerve head biomechanics. *Invest Ophthalmol Vis Sci*. 2004;45:4378–4387.
56. Del Priore LV. Stiffness of retinal and choroidal tissue: a surface wrinkling analysis of epiretinal membranes and choroidal folds. *Am J Ophthalmol*. 2006;142:435–440.
57. Wall M, George D. Idiopathic intracranial hypertension. A prospective study of 50 patients. *Brain*. 1991;114(pt 1A):155–80.
58. Corbett JJ, Savino PJ, Thompson HS, et al. Visual loss in pseudotumor cerebri. Follow-up of 57 patients from five to 41 years and a profile of 14 patients with permanent severe visual loss. *Arch Neurol*. 1982;39:461–474.
59. Burgoyne CF, Morrison JC. The anatomy and pathophysiology of the optic nerve head in glaucoma. *J Glaucoma*. 2001;10: S16–S18.
60. Sigal IA, Ethier CR. Biomechanics of the optic nerve head. *Exp Eye Res*. 2009;88:799–807.
61. Carta A, Favilla S, Prato M, Bianchi-Marzoli S, Sadun AA, Mora P. Accuracy of funduscopy to identify true edema versus pseudoedema of the optic disc. *Invest Ophthalmol Vis Sci*. 2012;53:1–6.
62. Bassi ST, Mohana KP. Optical coherence tomography in papilledema and pseudopapilledema with and without optic nerve head drusen. *Indian J Ophthalmol*. 2014;62:1146–1151.
63. Kulkarni KM, Pasol J, Rosa PR, Lam BL. Differentiating mild papilledema and buried optic nerve head drusen using spectral domain optical coherence tomography. *Ophthalmology*. 2014;121:959–963.
64. Sarac O, Tasci YY, Gurdal C, Can I. Differentiation of optic disc edema from optic nerve head drusen with spectral-domain optical coherence tomography. *J Neuroophthalmol*. 2012;32: 207–211.
65. Lee KM, Woo SJ, Hwang JM. Differentiation of optic nerve head drusen and optic disc edema with spectral-domain optical coherence tomography. *Ophthalmology*. 2011;118: 971–977.
66. Johnson LN, Diehl ML, Hamm CW, Sommerville DN, Petroski GF. Differentiating optic disc edema from optic nerve head drusen on optical coherence tomography. *Arch Ophthalmol*. 2009;127:45–49.
67. Merchant KY, Su D, Park SC, et al. Enhanced depth imaging optical coherence tomography of optic nerve head drusen. *Ophthalmology*. 2013;120:1409–1414.
68. Sato T, Mrejen S, Spaide RF. Multimodal imaging of optic disc drusen. *Am J Ophthalmol*. 2013;156:275–282.e1.

Investigative Ophthalmology & Visual Science

69. Flores-Rodriguez P, Gili P, Martin-Rios MD. Sensitivity and specificity of time-domain and spectral-domain optical coherence tomography in differentiating optic nerve head drusen and optic disc oedema. *Ophthalmic Physiol Opt*. 2012;32:213–221.
70. Murthy RK, Storm L, Grover S, Brar VS, Chalam KV. In-vivo high resolution imaging of optic nerve head drusen using spectral-domain optical coherence tomography. *BMC Med Imaging*. 2010;10:11.
71. Dignam K. Choroidal folds in association with optic disc drusen. *Clin Eye Vis Care*. 1997;9:99–107.
72. Fried MM-SG, Koch A. Excessive hypermetropia: review and case report documented by echography. *Ann Ophthalmol*. 1982;14.
73. Boldt HC, Byrne SF, DiBernardo C. Echographic evaluation of optic disc drusen. *J Clin Neuroophthalmol*. 1991;11:85–91.
74. Rubinstein K, Ali M. Retinal complications of optic disc drusen. *Br J Ophthalmol*. 1982;66:83–95.
75. Rosenberg MA, Savino PJ, Glaser JS. A clinical analysis of pseudopapilledema. I. Population, laterality, acuity, refractive error, ophthalmoscopic characteristics, and coincident disease. *Arch Ophthalmol*. 1979;97:65–70.

Appendix

OCT Substudy Committee for the NORDIC Idiopathic Intracranial Hypertension Study Group

Peggy Auinger, MS (University of Rochester School of Medicine & Dentistry, Rochester, NY, USA); Mary Durbin, PhD (Carl Zeiss Meditec, Inc., Dublin, CA, USA); Steven Feldon, MD, MBA (University of Rochester School of Medicine & Dentistry, Rochester, NY, USA); Mona K. Garvin, PhD (Iowa City VA Health Care System and the University of Iowa, Iowa City, IA, USA); Randy H. Kardon, MD, PhD (Iowa City VA Health Care System and the University of Iowa, Iowa City, IA, USA); John Keltner, MD (University of California, Davis, CA, USA); Mark Kupersmith, MD (OCT substudy principal investigator, Mount Sinai Roosevelt Hospital and New York Eye and Ear Infirmary, NY, USA); Patrick Sibony, MD (State University of New York at Stony Brook, NY, USA); Kim Cello (University of California, Davis, CA, USA); Jui-Kai Wang, MS (Iowa City VA Health Care System and the University of Iowa, Iowa City, IA, USA); John S. Werner, PhD (University of California, Davis, CA, USA).

IIHTT Acknowledgment List

Steering Committee: Michael Wall, MD (principal investigator, University of Iowa); James Corbett, MD, FAAN (University of Mississippi Medical Center); Steven Feldon, MD, MBA (University of Rochester Eye Institute); Deborah Friedman, MD (UT Southwestern Medical Center); John Keltner, MD (University of California, Davis, CA, USA); Karl Kieburtz, MD, MPH (University of Rochester School of Medicine & Dentistry); Mark Kupersmith, MD (OCT substudy principal investigator, Mount Sinai Roosevelt Hospital and New York Eye and Ear Infirmary, NY, USA); Michael P. McDermott, PhD (University of Rochester School of Medicine & Dentistry); Eleanor B. Schron, PhD, RN, FAAN (project offcer, National Eye Institute); David Katz, MD (Bethesda Neurology LLC); Tippi Hales (Raleigh Neurology Associates PA); Cindy Casaceli, MBA (University of Rochester School of Medicine & Dentistry).

Substudy Sites: New York Eye and Ear Infirmary: Rudrani Banik, MD (principal investigator); Sanjay Kedhar, MD (subinvestigator); Flora Levin, MD (Investigator); Jonathan Feistmann, MD (investigator); Katy Tai, MA (coordinator); Alex Yang, BA (cocoordinator); Karen Tobias, BA (coordinator); Melissa Rivas, BA (cocoordinator); Lorena Dominguez, BA (coordinator); Violete Perez, BA (coordinator). University of Iowa and Department of Veterans Affairs: Reid Longmuir, MD (principal investigator); Matthew Thurtell, MBBS, MSc (subinvestigator); Trina Eden (coordinator); Randy Kardon, MD, PhD (subinvestigator). The Eye Care Group: Robert Lesser, MD (principal investigator); Yanina ONeil, MD (subinvestigator); Sue Heaton, BS, CCRC (coordinator); Nathalie Gintowt (cocoordinator). Bascom Palmer Eye Institute, University of Miami: Byron L. Lam, MD (principal investigator); Joshua Pasol, MD (subinvestigator); Potyra R. Rosa, MD (coordinator); Alexis Morante, MS (cocoordinator); Jennifer Verriotto, MS (coordinator). Bethesda Neurology, LLC: David Katz, MD (principal investigator); Tracy Asbury (coordinator); Robert Gerwin, MD (subinvestigator); Mary Barnett (data entry). Swedish Medical Center: Steven Hamilton, MD (principal investigator); Caryl Tongco (coordinator); Beena Gangadharan (cocoordinator); Eugene May, MD (subinvestigator). Dean A. McGee Eye Institute: Anil Patel, MD (principal investigator); Bradley Farris, MD (subinvestigator); R. Michael Siatkowsk, MD (subinvestigator); Heather Miller, LPN (coordinator); Vanessa Bergman (cocoordinator); Kammerin White (coordinator); Steven ODell (lumbar puncture); Joseph Andrezik (lumbar puncture); Timothy Tytle (lumbar puncture). University of Pennsylvania: Kenneth Shindler MD, PhD (principal investigator); Joan Dupont (coordinator); Rebecca Salvo (coordinator); Sheri Drossner (cocoordinator); Susan Ward (coordinator); Jonathan Lo (Coordinator); Stephanie Engelhard (coordinator); Elizabeth Windsor (coordinator); Sami Khella (lumbar puncture); Madhura Tamhankar, MD (subinvestigator). Washington University in St. Louis School of Medicine: Gregory Van Stavern, MD (principal investigator); Jamie Kambarian (coordinator); Renee Van Stavern, MD (subinvestigator); Karen Civitelli (Regulatory); J. Banks Shepherd, MD (subinvestigator). University of Alabama Birmingham: Michael Vaphiades, DO (principal investigator); Jason Swanner, MD (investigator); A. Blane Jett (coordinator); Karen Searcey (coordinator); Frankie Webb (coordinator); Ashley Knight, BA (coordinator); Shereka Lewis, BS (coordinator); Lanning Kline, MD (subinvestigator); Ronald Braswell, MD (subinvestigator). Raleigh Neurology Associates, PA: Syndee J. Givre, MD, PhD (principal investigator); Tippi Hales (coordinator); Penni Bye (coordinator); Keisha Fuller (coordinator); Kenneth M. Carnes, MD, (subinvestigator); Kimberly James (regulatory); Marisol Ragland (data entry). St. Louis University: Sophia M. Chung, MD (principal investigator); Dawn M. Govreau, COT (coordinator); John T. Lind, MD, MS (subinvestigator). University of Rochester Eye Institute: Zoe Williams, MD (principal investigator); George OGara (coordinator); Kari Steinmetz (coordinator); Mare Perevich (coordinator); Karen Skrine (coordinator); Elisabeth Carter (coordinator); Rajeev Ramchandran, MD (subinvestigator). Ohio State University: Steven Katz, MD (Principal Investigator); Marc Criden, MD (investigator); Gina Coman, RMA, CPC, OCS (cocoordinator); John McGregor, FACS, MD, (subinvestigator); Andrea Inman (regulatory). Johns Hopkins University: Prem S. Subramanian, MD, PhD (principal investigator); Paul N. Ho_man, MD, PhD (investigator); Marianne Medura (coordinator); M. Michaele Hartnett (coordinator); Madiha Siddiqui (coordinator); Diane Brown (coordinator); Ellen Arnold (cocoordinator); Jeff Boring, MD (subinvestigator); Neil R. Miller, MD (subinvestigator). University of Southern California: Peter Quiros, MD (principal investigator); Sylvia Ramos (coordinator); Margaret Padilla (coordinator); Lupe Cisneros (coordinator); Anne Kao, MD (subinvestigator); Carlos Filipe Chicani, MD (subinvestigator); Kevin Na (regulatory). University of Houston: Rosa Tang, MD, MPH, MBA (principal investigator); Laura Frishman, PhD (coordinator); Priscilla Cajavilca, MD (coordinator); Sheree

Investigative Ophthalmology & Visual Science

Newland, LVN (coordinator); Liat Gantz, OD, PhD (coordinator); Maria Guillermo Prieto, MD (coordinator); Anastas Pass, OD, JD (coordinator); Nicky R. Holdeman, OD, MD (subinvestigator). University of Calgary: William Fletcher, MD, FRCPC (principal investigator); Suresh Subramaniam, MSc, MD, FRCPC (investigator); Jeannie Reimer (coordinator); Jeri Nickerson (coordinator); Fiona Costello, MD, FRCPC (subinvestigator). The Greater Baltimore Medical Center: Vivian Rismondo-Stankovich, MD (principal investigator); Maureen Flanagan, CO, COA (coordinator); Allison Jensen, MD (subinvestigator). State University of New York at Stony Brook: Patrick Sibony, MD (principal investigator); Ann Marie Lavorna, RN (coordinator); Mary Mladek, COT (coordinator); Ruth Tenzler, RN (coordinator); Robert Honkanen, MD (subinvestigator); Jill Miller-Horn, MD, MS (lumbar puncture); Lauren Krupp, MD (lumbar puncture). Massachusetts Eye and Ear Infirmary: Joseph Rizzo, MD (principal investigator); Dean Cestari, MD (subinvestigator); Neal Snebold, MD (investigator); Brian Vatcher (coordinator); Christine Matera (coordinator); Edward Miretsky, BA (coordinator); Judith Oakley, BA (coordinator); Josyane Dumser (coordinator); Tim Alperen, BA (coordinator); Sandra Baptista-Pires (coordinator); Ursula Bator, OD (coordinator); Barbara Barrett, RN (coordinator); Charlene Callahan (coordinator); Sarah Brett (coordinator); Kamella Zimmerman (coordinator); Marcia Grillo (coordinator); Karen Capaccioli (coordinator); Duke Eye Center and Duke University Medical Center M. Tariq Bhatti MD (principal investigator); LaToya Greene, COA, CRC (coordinator); Maria Cecilia Santiago-Turla (coordinator); Noreen McClain (coordinator); Mays El-Dairi MD (subinvestigator); Florida State University College of Medicine: Charles Maitland, MD (Principal Investigator); H. Logan Brooks Jr, MD (investigator); Ronda Gorsica (coordinator); Brian Sherman, MD (subinvestigator); Joel Kramer, MD (subinvestigator); William Beaumont Hospital: Robert Granadier, MD (principal investigator); Tammy Osentoski, RN (coordinator); Kristi Cumming, RN (coordinator); Bobbie Lewis, RN (coordinator); Lori Stec, MD (subinvestigator)

Dietary Weight Loss Program: Betty Kovacs; Richard Weil, MEd, CDE; Xavier Pi-Sunyer, MD (New York Obesity Nutrition Research Center).

Fundus Reading Center: William Fisher, Dorothea Castillo, Valerie Davis, Lourdes Fagan, Rachel Hollar, Tammy Keenan, Peter MacDowell (University of Rochester Eye Institute).

Visual Reading Field Center: John Keltner, MD; Kim Plumb; Laura Leming (UC Davis Department of Ophthalmology & Vision Science); Chris Johnson (University of Iowa).

Optical Coherence Tomography Reading Center: John Keltner, MD; John S. Werner, PhD; Kim Plumb; Laura Leming (UC Davis Department of Ophthalmology & Vision Science); Danielle Harvey, PhD (UC Davis Department of Public Health Sciences, Division of Biostatistics).

Data Coordination & Biostatistics Center: Jan Bausch, BS; Shan Gao, MS; Xin Tu, PhD (biostatistics); Debbie Baker; Deborah Friedman, MD, MPH (medical monitor); Karen Helles; Nichole McMullen; Bev Olsen; Larry Preston; Victoria Snively; Ann Stoutenburg (CHET/CTCC; University of Rochester School of Medicine & Dentistry).

NORDIC Headquarters: O. Iyore Ayanru, Elizabeth-Ann Moss, Pravin Patel (Mount Sinai Roosevelt Hospital). Consultant: Richard Mills, MD (Glaucoma Consultants Northwest).

Data Safety Monitoring Board Members: Maureen Maguire, PhD (chair, University of Pennsylvania); William Hart Jr, MD, PhD; Joanne Katz, ScD, MS (Johns Hopkins); David Kaufman, DO (Michigan State University); Cynthia McCarthy, DHCE MA; John Selhorst, MD (St. Louis University School of Medicine).

Adjudication Committee: Kathleen Digre, MD (University of Utah); James Corbett, MD, FAAN (University of Mississippi Medical Center); Neil R. Miller, MD (Johns Hopkins University); Richard Mills, MD (Glaucoma Consultants Northwest).

Investigative Ophthalmology & Visual Science